

Temperature regulation for thermoplastic micro-forming of bulk metallic glass: Robust control design using buck converter[☆]

Nattasit Dancholvichit*, Shiv G. Kapoor, Srinivasa M. Salapaka

University of Illinois Urbana-Champaign, United States

ARTICLE INFO

Keywords:
 Robust control
 Manufacturing process
 Process control
 Micro-forming
 Temperature control
 Buck converter

ABSTRACT

This article presents the design, identification, simulation, and control of a buck converter implemented for bulk metallic glass thermoplastic micro-forming. In manufacturing of multi-faceted bulk metallic glass knife edge, the temperature of the micro-forming sample is critical to the thermoplastic deformation, which determines the quality of the blade edge shape. We propose a nested inner-current outer-temperature control system for high-fidelity temperature regulation. The inner-current control loop is implemented on a modified buck converter, which allows high-power rectified AC input and outputs current that can be regulated with a precision of 2 % over a bandwidth of 5 Hz. We use switch-averaged electrical model together with feedback linearization to address complex nonlinear dynamics that describe a buck converter, and to enable it using linear control design methods. The outer-temperature control design ensures temperature regulation of a heater by prescribing real-time reference power that the current-control loop should provide. The challenge of nonlinear relationship between the required reference power and the regulated current is addressed by exploiting the high-bandwidth of the inner-current loop. The control objectives of regulation performance and robustness to modelling uncertainties are posed and solved in an optimal control (H_∞) framework. Experimental results demonstrate that our control design achieved the required temperature regulation at 673 K within 0.03 K. An improvement of over 5000 % is demonstrated when compared with previously implemented control designs. Moreover, the buck converter-based system enables regulation accuracies that were not possible with other popular existing methods such as TRIAC and traditional relay switches.

1. Introduction

In corneal surgery, higher quality blades result in shorter recovery time, less trauma to the eye, and reduced possibility of repercussion. Vitreloy-1 [1], a zirconium-based bulk metallic glass (BMG) with chemical formula: $Zr_{41.2}Ti_{13.8}Cu_{12.5}Ni_{10.0}Be_{22.5}$, is shown to be an alternative material for manufacturing the surgical blade [1–4]. At temperatures above their glass transition temperature, BMG samples can undergo thermoplastic drawing and molding process, which can result in formation of sharp-edged blades. At room temperature, BMG has high strength and hardness that are ideal for the formation and retention of sharp edges. Krejcie [2] successfully developed a testbed for BMG thermoplastic forming that can manufacture straight edge surgical blades with an edge radius of 50 nm. Zhu [3] later developed another testbed that can successfully manufacture high-quality sharp curvilinear edge surgical blades. From these previous studies, it is found that the blade quality is very sensitive to the temperature during the forming

process. Slight fluctuations of the temperature can alter the type of deformation of BMG [4] from homogeneous deformation in the Newtonian region to high viscosity deformation in the Non-Newtonian region, which yields poor quality edges of the blades [2,3]. For a better understanding of the drawing process Dancholvichit et al. [4] developed an Auto-Regressive eXogenous, ARX model for predicting the process temperature and implemented fuzzy logic control based on these models. Here, it was shown that the steady state error in temperature regulation in their setup mainly stems from the modelling uncertainties in the temperature process. The control design improved the root mean square error, RMSE to ± 2.5 K for the referenced temperature setup of 673 K. However, the steady state error of the controller is limited by relatively low bandwidth from relay switches. A new control architecture is needed to achieve precise temperature regulation and to address the inconsistency of the manufactured blade edges.

In most resistive heating control applications, there are several

* 48th SME North American Manufacturing Research Conference, NAMRC 48, Ohio, USA.

[☆] Corresponding author.

E-mail address: danchol2@illinois.edu (N. Dancholvichit).

approaches that control the temperature. Many of them use relay switches where pulse width modulation (PWM) signals are used to appropriately turn on/off the power sources so that the average power over a period is as required by the load. Recently solid-state type relay switches are becoming more popular since with these devices it is possible to increase the switching frequency without wearing the components. Liu et al. in [5] used a relay-based system for temperature control of injection molding machine, where temperature load disturbances were addressed using system identification and internal-model-principle based control. However, relay switches cannot provide consistent power output over control cycle, which is possible only when switching frequency is much higher than the frequency of the AC source. Several heating and lighting applications use Triode for alternating current (TRIAC) circuits, where phase of the AC cycle is appropriately controlled with zero crossing detector sensing made possible from the opto-coupler, and the power input to the heater is controlled by the firing synchronized pulses of PWM signal from the controller. However, this circuit cannot provide high power factor and still has power fluctuation within an AC time period. As a result, the bandwidth of the controller is limited to the frequency of the AC source and it requires a setup of opto-coupler to detect zero-crossing, which makes it an unattractive option [6]. Liu et al. proposed an AC chopper circuit that uses insulated gate bipolar transistor (IGBT) to appropriately condition the power from the AC source and obtain controllable average power output [7]. Moon et al. also proposed a similar idea but implemented the AC chopper to the buck converter [8]. Baharom et.al. modified the AC to AC converter circuit using single phase matrix converter configuration [9]. For these studies, the output signal is not in the continuous mode and has high fluctuations as high as the amplitude of the AC input source. Finally, DC power supply could also be an alternative approach that convert the power from AC mains to high power DC. The heater can be regulated using DC controller [10], but the related setup and instrument costs are much higher since the heating applications consume higher current relative to other types of load.

This article presents a hardware design along with the control framework that enables temperature regulation required for drawing process for BMG. It is very critical that BMG is regulated within a small temperature window in order to provide predictable thermoplastic forming behaviour required for sharp blades with low edge radius. The primary control objectives are to regulate the temperature within an error bound of 1.5 K. Such a design would ensure that the viscosity of the sample during thermoplastic drawing is within less than 2% of the desired value required for drawing BMG [2,3]. One of the primary challenges to achieving the temperature regulation is the complex dynamics that describes the drawing process, the modelling uncertainties especially in terms of convection, conduction, and radiation losses to air, and the stringent accuracy requirements on temperature regulation. The challenges on the hardware design include developing a system that can achieve temperature regulation within tight bounds while also satisfying low investment cost. Accordingly, we have developed a resistive heating system where the current is controlled precisely, thereby enabling precise thermal outputs and consequently tight temperature regulation. A heater system based on buck converter where the high-voltage power input from a rectified AC power source is converted to a low-voltage high current output as required. The innovations are in terms of enabling using AC source from the wall outlet in this implementation to minimize the cost of the setup. Also, typical existing buck converter designs do not provide high current outputs as required by our application; our circuit design makes it possible to achieve high current on the order of 2.5 amps with 300 W. The demands on the hardware and control design are to ensure that the transient overshoots in current are small, the current should be within saturation limits, and the closed-loop bandwidth of the combined electrical-thermal system is at least greater than 0.1 Hz.

The testbed configuration of the setup, electrical, and thermal

systems, and the overall control framework is discussed first, followed by the discussion of system identification of both systems. The simulation and robust control of both systems are then presented. Finally, the results and conclusions drawn for this study are given.

2. Testbed hardware and model

The hardware for the testbed comprises of the electrical system, the thermoplastic micro-forming platform, and the associated control hardware. The electrical system comprises of a buck converter and additional circuitry required for taking power from the wall AC source and regulating the current as required by the resistive heaters. BMG sample is drawn using the micro-forming platform. The control hardware takes in voltage and current sensor measurements from the electrical system and the temperature measurements from the micro-forming platform, and provides the on/off duty cycle for the buck converter, so that appropriate current is delivered to the heaters; thereby achieving temperature regulation required for drawing BMG. This section presents the testbed configuration, the electrical and thermal systems, and the layout of the control framework respectively.

2.1. Thermoplastic micro-forming testbed configuration

The testbed used in this study is a hybrid thermoplastic micro-forming process discussed in [3,5]. The setup of the machine is shown in Fig. 1(a). The machine consists of a lever arm mechanism driven by a vertical linear motor. This lever arm is connected to the molding module that can exert the amplified force from the linear motor to the BMG sample. There are two drawing modules, offset by 90°, located in the front of the molding module. These two modules, which are voice coil actuated enable micro-drawing of the sample horizontally to create blade edges. Molding and drawing dies, which attach to the corresponding modules are connected to the heater cartridges.

There are six resistance detectors (RTD) installed near each of the six heater cartridges; two on top and bottom dies (RTD1 and RTD2) and four on each grip (RTD3 and RTD4 on the left and RTD5 and RTD6 on the right), respectively as shown in Fig. 1(b) and (c) [3,5]. In our design, we assume that the temperature measurements from the RTDs

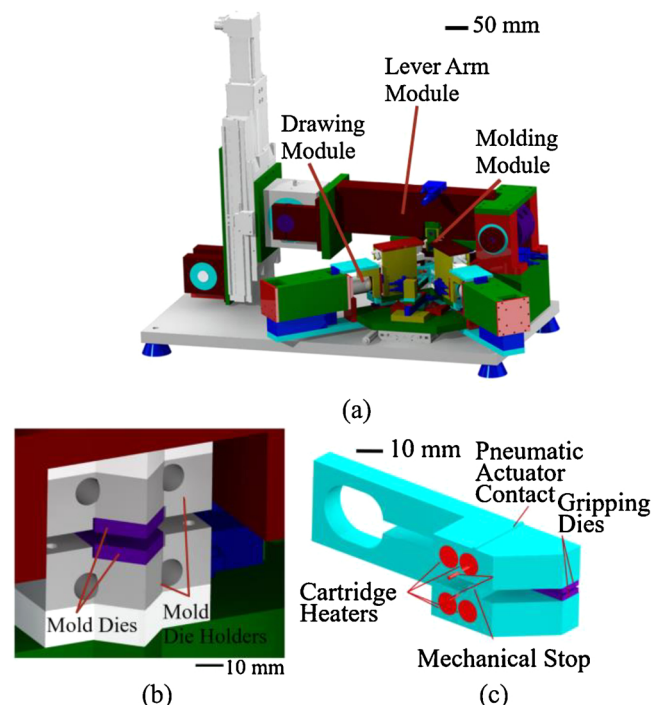


Fig. 1. Configuration of thermoplastic forming testbed [3].

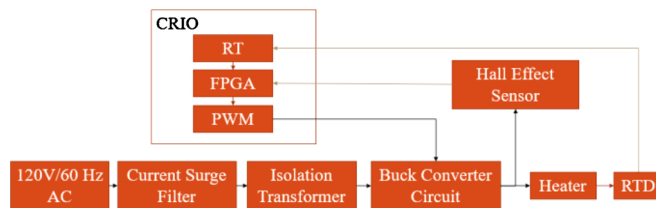


Fig. 2. Hardware diagram of components.

approximate well the temperatures of the respective dies since the distances between them is small and heat is applied to the center of the six heaters. The electrical current passing through heater cartridges is measured by the hall-effect current sensor. The control signal is generated from a field programmable gate array (FPGA) from the CompactRIO 9074 by LABVIEW with 8 C-series modules that have I/O interface to control various actions of the process. There are three sub-systems involved. Two NI 9217s are used to measure six temperature measurements including molding and drawing module of the testbed, a NI 9472 is used to send PWM digital signal of temperature controller and a NI 9205 receives current feedback from the hall effect sensor, HX03-P. The real-time (RT) processor is embedded in the compactRIO hardware processing within a deterministic operating system along with FPGA unit that computes time critical tasks.

The hardware components for the temperature control is illustrated in Fig. 2. The 120 V/60 Hz AC source is first filtered and isolated from the earth ground using a transformer before connecting to the buck converter. Buck converter receives the controlled PWM signal generated from FPGA in LABVIEW. In this paper, we are demonstrating one heater control (RTD3) but the design is scalable to all the six heaters. Initial calibration of the PWM algorithm that generates PWM signal to the IGBT is performed.

The output of the buck converter is an electrical current that can be controlled by appropriately designing the duty cycle $D(t)$. The electrical current passing through a resistor generates the power consumed by the heaters that can be measured by RTD. The temperature value from RTD is then transferred back to the RT in LABVIEW. The calibrated temperature data from RTD sensors are fed to the control algorithm in RT resource. The current reference is passed through the electrical control loop to evaluate $D(t)$ in FPGA. The implemented duty cycles need to be calibrated in order to ensure the precise PWM in IGBT from FPGA. This calibration is to compensate the offset voltage of IGBT, response time of the PWM unit, and voltage drop across the IGBT [11]. From the experimental calibration, $D_g(t)$ and $D(t)$ are related as $D(t) = 1.0181D_g(t) - 0.1569$ with $R^2 = 0.99$.

2.2. Electrical system

The main component of the electrical system is the buck converter. Buck converters belong to a class of switched-mode power electronics, where a semiconductor based high frequency switching mechanism (and associated electronic circuit) connected to a DC power source enables changing voltage and current characteristics at its output. A buck-converter regulates a voltage at its output, which is smaller (and hence higher current) than the input voltage. The circuit diagram of a general buck converter is given in Fig. 3(a). The output voltage/current is achieved through designing the duty-cycle of the switching component, how long the switch is on or off during a switch cycle; this design is implemented using an appropriately designed PWM signal. When the switch Q (implemented using an IGBT) is in the *on* state, there is no current through the diode and the current flows through the inductor and the load. When it is on the *off* state, the current then free-wheels and slowly decays from the capacitor through diode and the load. The frequency of the switch and the inductance is chosen so that the current through inductor would not drop to zero; that is to maintain

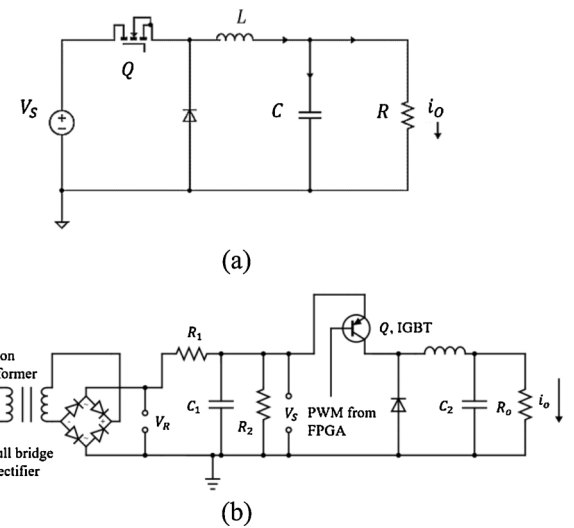


Fig. 3. Buck converter circuit (a) and modified buck converter (b) schematic.

it in continuous-current-mode (CCM).

The heating system requires high-power over a long time that typical cheap dc sources cannot provide. Therefore, in our work, we modify the buck-converter circuit by appending a rectifying circuit that takes in AC power from a wall outlet and provides the corresponding DC power to the buck converter. Fig. 3(b) shows a schematic of the modified circuit. This switch-based circuit takes the AC input from the 120 V/60 Hz AC wall outlet. The bridge rectifier converts AC source to rectified sinusoidal DC signal. The resistors and capacitor attenuate the ripple of the rectified DC before passing to the IGBT. The rectified voltage, V_s , is input to the buck converter, which is controlled by IGBT. The modification of this buck converter is on the right side of the schematic, where the AC source is rectified and smoothed out by a set of low pass filter with R_1 and C_1 . This results in lower output power compared to the AC from the wall. Another resistance R_2 is attached in parallel to the capacitor C_1 which makes it possible to dissipate the energy out when the circuit is switched off. The output of the circuit is i_o which is the current passing through the heater, R_o . The buck converter in this application is designed to be operated in continuous current mode to prevent nonlinearity and discontinuous current.

To model this circuit, we determine dynamics of the buck converter averaged over a switch cycle. Here we exploit that the switching frequency is much faster (~ 10 kHz) than the desired bandwidth of the closed-loop system (~ 30 Hz). The averaged model neglects the high frequency dynamics, but it is sufficient as the bandwidth of the controller is much slower than the pulse frequency of the switching cycle. The averaged dynamic model of a buck converter is given by;

$$L \frac{d(i_L(t))}{dt} = D(t)V_s(t) - i_o(t)R \quad RC_2 \frac{di_o(t)}{dt} = i_L(t) - i_o(t), \quad (1)$$

where $i_L(t)$ is the current through the inductor, $i_o(t)$ is the output current, $D(t)$ represents the duty-cycle of the input at time t . $V_s(t)$ is the voltage across IGBT [9,10,12].

In the modified circuit, $V_s(t)$ is the voltage across IGBT which can be derived from the appended circuit as;

$$C_1 \frac{dV_s(t)}{dt} = \frac{V_R(t)}{R_1} - \left(\frac{1}{R_1} + \frac{1}{R_2} \right) V_s(t) - D(t)i_L(t), \quad (2)$$

where $V_R(t)$ is the voltage across the bridge rectifier.

Note that the modified circuit is described by Eqs. (1) and (2) are coupled, nonlinear and it is relatively difficult to design the duty cycle $D(t)$ to make $i_o(t)$ track a prescribed reference signal. To simplify control design, we exploit the structure of these equations and available hardware. First, we redefine the control variable by $u(t) = D(t)V_s(t)$.

Table 1
Component parameter values in the proposed circuit.

Components	Value (units)
L	4.8 mH
R_o	47.2 Ω
R_1	14.4 Ω
R_2	10 kΩ
C_1	470 μF
C_2	100 μF
L_q	13 nH
R_q	5 Ω

This makes the system of Eq. (1) a linear control system, where the system dynamics is linear in the control design variable u . Now we place a voltage sensor that measures $V_s(t)$, which has multiple benefits: (a) The duty cycle $D(t)$ is easily determined in terms of the control design variable $u(t)$ and measurement $V_s(t)$ simply by $D(t) = \frac{u(t)}{V_s(t)}$; (b) It makes the control design independent of the more complicated dynamics for V_s given by Eq. (2). We have to ensure that the control design is such that $V_s(t)$ is not unreasonably high; (c) These modifications result in a simple linear-time invariant control system, which enables obtaining simple models through system identification. More precisely, the transfer function between input $u(t)$ and output $i_o(t)$ is determined from frequency response. These empirical models are more accurate than the model given in Eqs. (1) and (2) since they capture uncertainties such as parasitic resistances not modeled by Eq. (1); and (d) It enables robust optimal control design - here we can account for multiple sources of modeling uncertainty, which includes sensor noise in measurements of voltage $V_s(t)$.

The parameters of the components used in the setup are listed in Table 1. The selection of the hardware components is based on the resistance value of the heater, R_o . Resistance R_1 is chosen such that it lowers the maximum current going to the heater, since the power required at the resistor R_o to maintain a desired temperature is significantly lower than the input AC power. Addition of capacitor C_1 completes the low pass filter configuration and ensures that the ripples in the rectified voltage V_s is attenuated. R_2 helps dissipate the surplus power when the circuit is not used and turned off. L and C_2 are chosen to maintain the circuit to be in continuous mode. High value of L ensures that the current after IGBT does not cross zero and C_2 is to minimize ripple of the current output.

This design that incorporates buck converter and low pass filter provides the current output to be controlled in any desired shape since the output is the continuous DC signal. The advantage of this proposed buck converter design is that the output current is not chopped discontinuously as presented in many existing approaches [6–9]. Using relay switches alone in hard switching mode also results in chopped sinusoidal wave; here the power is not transferred to the heater efficiently due to hard switching interrupting the power during zero crossing of the current. It is also harder to control with nonlinear response introduced by the relay switch. Similarly, the TRIAC circuit provides chopped current output in every AC cycle which in turn limits the maximum current tracking bandwidth to be the frequency of the AC cycle. The proposed design here can track the referenced current in any desired shape since it provides continuous current output. The energy loss to switches is minimized due to no zero crossing during operation. In addition, the drawing process can benefit from this design, where the temperature can be varied along the length of the extrusion during the sample drawing process.

2.3. Thermal system

The thermal system is operated by cartridges heater made of resistive heating element that converts electrical power to thermal power. The thermal output power is proportional to the electrical input power

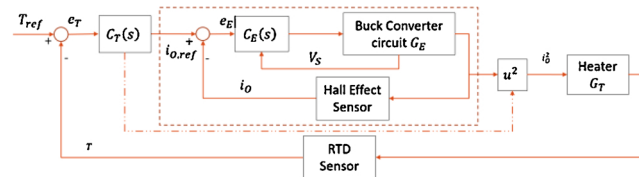


Fig. 4. Block diagram representation of the inner-outer control design.

with an efficiency factor γ , that is, $P_{\text{thermal}} = \gamma(i_o^2 R)$ based on Joule-Lenz law. In this work we use DC current input to regulate the temperature of the module. The RTD sensor is a 100 Ω wire-wound type that provide feedback to the DAQ with a resolution of 3E-3K. In our design, we assume that the temperature coefficients of all resistors are negligible, including all the resistive heaters. As a result, all resistances in the circuit are constant and not a function of temperature. The heating module along with RTD sensor could be viewed as a large complex dynamic plant with model uncertainties including convection, conduction, and radiation losses to air. We use system identification to estimate the dynamics of the heating module. With fast-response current control from the electrical system provided to the thermal system, precise temperature can be obtained since the controller is designed to reject the disturbances and compensate for the model uncertainties.

2.4. Control framework and limitations

The complexity of the dynamics of coupled electrical and thermal systems is addressed by employing a nested structure in the control framework. This nested structure comprises an inner-current feedback loop and an outer-temperature feedback loop as shown in Fig. 4. This structure exploits the difference in temporal bandwidth of the *fast* electrical and the *slow* thermal systems. The faster inner-current loop tracks the reference input current as prescribed by the outer-temperature loop and outputs electrical current feedback going to the heater, G_T . The inner loop controller G_E , is implemented by designing appropriately the duty cycles for the proposed buck converter, G_E described in Section 2.2. The slower outer loop is the temperature controller G_T , is designed such that it provides an appropriate input power P regulates the temperature at a prescribed reference value. The required power input from the outer-loop control design is provided by the electrical power from the buck-converter circuit. Accordingly, the desired current, $i_{o,\text{ref}}$ from the inner loop is designed so that $P = \gamma i_{o,\text{ref}}^2 R$.

By principle of Joule heating, thermal power is provided by the electrical current flows through ohmic conductor [13]. The stability of these two interconnected systems can be analyzed using slow and fast manifolds of singular perturbation model [14]. The thermal system is a slow dynamic system, which is of the form $\dot{x}_T = A_{11}x_T + b_1 P; T = c_T x_T$ (3). The fast system, $\dot{x}_e = A_{22}x_e + b_2 u; i_o = c_2 x_e$ (4) represents the electrical system. The nonlinearity given by $P = \gamma R_o i_o^2$ arises from the interface between these two systems, where γR_o is a constant. From singular perturbation theory (Theorem 11.1 from [14]), we know that $\|x_\varepsilon^*(t) - \bar{x}(t)\|$ is $O(\varepsilon)$, where $x_\varepsilon^*(t)$ and $\bar{x}(t)$ represent the solutions of the above set of differential equations for $\varepsilon = \varepsilon^*$ and $\varepsilon = 0$. We estimate that ε is on the order of $\frac{\omega_T}{\omega_E} \approx 10^{-4}$. This justifies using $\varepsilon = 0$ for our control design, which in turn corresponds to using the inner-outer cascaded structure where we disregard the dynamics of the current-loop and can assume that $P = \gamma R_o i_{o,\text{ref}}^2$, when considering the time-scales of the thermal system. As a result, we design each controller separately and combine them together during the implementation. i_o feedback from the inner control loop then passes through the heater which its temperature measured by RTD sensor described in 2.1 and 2.3 and complete the feedback to the outer loop.

The two controllers are implemented in two different sections of the DAQ. Since the inner control loop are more time critical, it is implemented using in FPGA portion of the DAQ. The temperature controller is implemented in a relatively slower RT signal processor and

then fed back to FPGA for the buck converter controller. This allows us to distribute some computational load to RT from FPGA. It is noted that there is negligible delay between data transfer between the two loops.

Apart from the designing the control law, the controller must be designed under practical and fundamental limitations, especially stemming from the constraints in the hardware implementation. The controlled signal needs to be within saturations limit of the controller and does not exceed the range and precision of the fix point data during implementation in FPGA. The data acquisition rate and the delay between control loop needs to be minimized. Finally, the sampling frequency of the discretized controller are more than 30 times the frequency range of operation [15].

3. System identification of the electrical and thermal systems

To obtain the required dynamic models of the component systems, the system identification for both the electrical and thermal systems are carried out in this section.

3.1. System identification and verification of the electrical system

The dynamics of the buck converter circuit is obtained by determining the transfer function from $u_E(t) = D(t)V_s(t)$ to the output $i_o(t)$. Line search with frequency-sweep identification in MATLAB called “tfest” toolbox is used. The input signal, $u_E(t) = 40 + A_E \sin(\omega t)$, with frequencies of 0–1000 Hz is given to the system for the experimental identification. Here the amplitude, $A_E = 15 V$, is considered sufficient so that the system is properly excited. The signal is also under saturation of the circuit to prevent electrical damage. An offset value of 40 is selected such that the current output of 1.16 A at the operating point of interest. This current would maintain the temperature of 673 K, the thermoplastic forming temperature of BMG. The data collected is split into 80 % for fitting the model and the other 20 % for validation. The transfer function of the buck converter from input to current output as obtained from our frequency response experiments is;

$$G_E(s) = \frac{36423(s + 5.032)(s + 0.02768)}{(s + 2837)(s + 820.8)(s + 3.797)(s + 0.02213)} \quad (3)$$

The response data from the sinusoidal input signal is compared with the identified controllable plant, G_E . The frequency response of the electrical system from averaged model, simulation and system identification are presented in Fig. 5. For the averaged model, the peak at 1440 rad/s is more noticeable than the other two models. This is due to the addition of the parasitic inductance, L_q , and resistance, R_q , of IGBT model [6,15]. However, there are other parasitic components embedded in all electronics components that makes the system more damped. As a result, the model from system identification is the most damped compared to the other two. We found that change in operating point from 20 to 50 V of the input signal has no significant effect to the

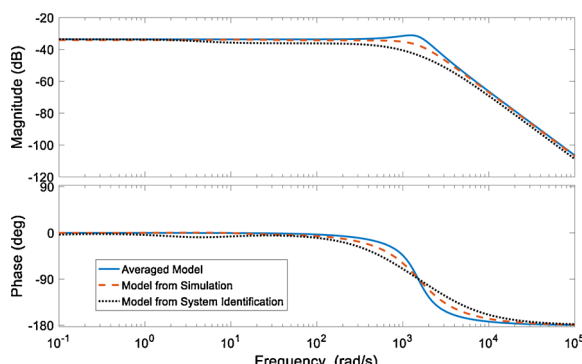


Fig. 5. Frequency response of the electrical system from averaged model, simulation and system identification.

results. For control design, we used the model derived from the system identification.

3.2. System identification of the heater

We again used frequency-response based system identification to derive the transfer function from the input i_o^2 to the output temperature as measured by RTD. Note that since $P_{thermal} = \gamma(i_o^2 R_o)$, we choose i_o^2 as a measure of input power, whereby the constants γ and R_o are embedded in the DC gain. Since power of the thermal temperature is proportional to the rate of change in temperature, the output temperature must have an integrator to obtain temperature. The system identification is forced to have $s = 0$ at one of the poles in the model. RTD raw data is also passed through lowpass filter with cutoff of 5 Hz to attenuate switching noise coming from IGBT.

The input signal, $u_T(t) = 1.35 + A_T \sin(\omega t)$, with frequencies of 0–20 Hz is given to the heater for identification. The operating point 1.35 is chosen so that it provides the molding temperature of 673 K, which is required for good quality blades. Amplitude, $A_T = 0.3A^2$, is sufficient such that the system is properly excited to a small temperature window of interest at ± 10 K. Two sets of input-output experimental data are collected. The first set is used to estimate the transfer function using “tfest”, similar to the electrical case. The first set of data is used to estimate the model and the second portion is for verification. The transfer function between the square of the electrical current and the temperature is estimated as;

$$G_T(s) = \frac{0.51414(s + 0.08723)}{(s + 0.02853)(s^2 + 0.1905s + 0.01352)} \quad (4)$$

The frequency response shown by Bode plots of the heater can be found in Fig. 6. The response data from the sinusoidal input signal is compared with the identified plant, G_T . We found that change in steady state operating point of the input signal has no significant change at temperature window of interest at up to ± 20 K. Hence, only one operating point of the heater is sufficient for the control analysis. We find that the relationship of the square of the current input to the temperature output of the heater is linear if the range of operation is in a small window.

4. H_∞ controller design

Both the thermal and the electrical systems have to meet multiple objectives of precise tracking of reference inputs, avoiding input saturation, and being robust to undesired dynamics. We used H_∞ control design since it is well suited to simultaneously design for multiple objectives. In this design, an optimization problem is posed that reflect these closed-loop objectives; the solutions to which is easily obtained using standard software routines (e.g. hinfss in Matlab). The frequency ranges of interest of different objectives are designed in terms of

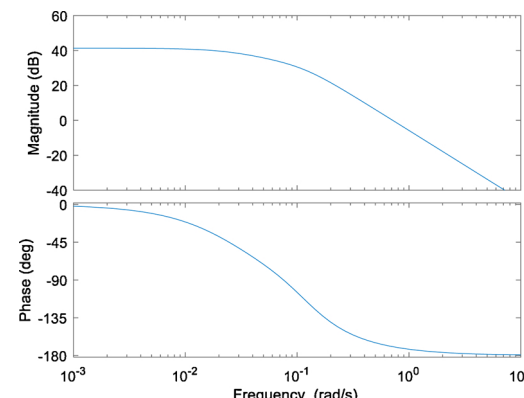


Fig. 6. Frequency response of the heater module.

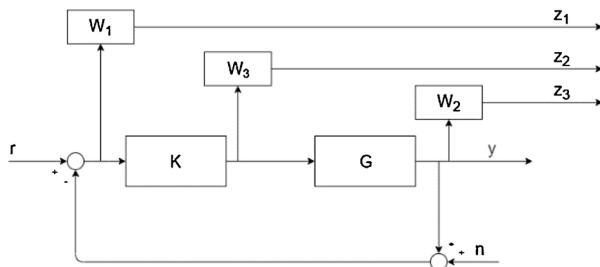


Fig. 7. Block diagram schematic for the robust control of both electrical and thermal systems.

weight transfer functions described below. In contrast to traditional PID control design, this design requires no tuning, once the objectives are precisely known. Here the controller order is the same size of the physical system (the plant); hence it is not limited by only few designable parameters as in PID design. It does result in higher-order controllers; however, in our case, it is not difficult to implement them in FPGA since the controller can be reduced and grouped into biquad filters.

H_∞ controllers are implemented on both buck converter and heater in order to meet specifications. Both controller choices and weighting functions are picked during the simulation and design phase in MATLAB. The design, testing and implementation of each controller will be performed separately and ensured that the controlled bandwidth frequency is not overlapping. We then can implement both controller into a system controller loop as discussed in control framework.

Fig. 7 demonstrates a block diagram, which can represent either of the electrical or thermal feedback control systems. Since we use the same principles for control design of both the systems, we present our design in terms of this general block diagram. Here, G represents the physical system (electrical or thermal system); r represents the referenced signal that the output y of the system G needs to track, d represents the dynamics effect of the disturbance – the effect of dynamics that have not been modelled by G ; and n is the sensor noise. The main objective of the controller is to minimize the tracking error, $e = r - y$.

For given controller K in a feedback-only configuration, the tracking error is given by;

$$e = r - y = S(r - d) + Tn, \quad (5)$$

where the sensitivity transfer function $S = (1 + GK)^{-1}$ and the complementary sensitivity transfer function $T = 1 - S = GK(1 + GK)^{-1}$. Hence, the tracking error is contributed from these two transfer functions. Note that there are some fundamental limitations, that is, there are some objectives that cannot be achieved irrespective of the control design. For instance, an important limitation arises from the algebraic constraint $S(j\omega) + T(j\omega) = 1$, which implies that $|S(j\omega)|$ and $|T(j\omega)|$ cannot be simultaneously made small at the same frequency range ω . Therefore, there is a tradeoff in deciding the frequency ranges where S and T can be made small. The performance of both plants is mainly characterized by robustness to modelling uncertainties and tracking bandwidth. The attenuation of the sensor noise n is addressed by designing K such that $|T(j\omega)|$ is small over the frequencies beyond a bandwidth ω_T . The tracking bandwidth, ω_{BW} , is determined by the range of frequencies over the magnitude plot of the sensitivity transfer function. This measure of bandwidth is used instead of the bandwidth obtained from T , ω_T since the actual response of the output is more related to S rather than T . The contribution of S and T must be balanced in such a way that the controller is able to minimize the tracking error without sacrificing ability to attenuate noise and maintain robustness requirements.

To set up the H_∞ optimization problem, we first identify the set of inputs and outputs. In this system, as shown in Fig. 7, the exogenous input w is the reference signal r . The control input is signal u and the error is signal e . In this work, we select 3 weighted functions to reflect

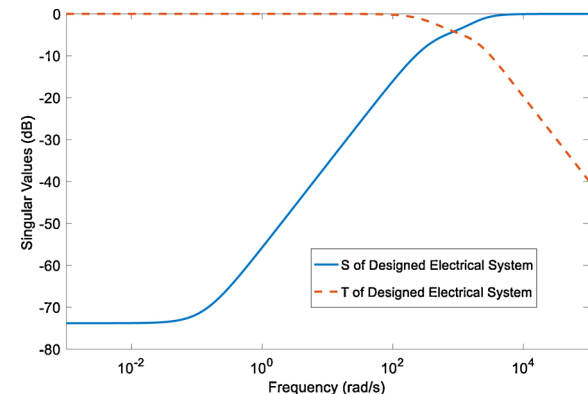


Fig. 8. S and T transfer function of electrical systems.

the performance objectives and physical constraints as shown in block diagram, Fig. 8. Three outputs, z_1 , z_2 , and z_3 correspond to weighted functions namely, W_1 , weighted tracking error, W_2 , weighted system output, and W_3 , weighted control input. The weighting functions imposes the bound on the bandwidth of the desired requirements and constraints. The transfer function $W_1 S$ characterizes the performance objective of good tracking error in output current. $W_2 T$ is the complementary transfer function that limit control gain at high frequency and output current tracking. $W_3 K S$ is to limit the control effort, $u(t)$, from saturation.

The setup the robust controller problem is to first construct the stacked H_∞ optimization problem [16]. The generalized plant, P can be augmented from the transfer function from exogenous inputs and auxiliary control input $w = [r, u]^T$ to regulated output $z = [z_1, z_2, z_3, e]^T$ given by;

$$\begin{bmatrix} z_1 \\ z_2 \\ z_3 \\ e \end{bmatrix} = \begin{bmatrix} W_1 & -W_1 G \\ 0 & W_2 G \\ 0 & W_3 \\ I & \underbrace{-G}_{=P} \end{bmatrix} \begin{bmatrix} r \\ u \end{bmatrix} \quad (6)$$

The optimization problem is to find controller K such that the H_∞ -norm of the above transfer function from w to z is minimized. W_1 is chosen to be large in frequency range to minimize tracking error. It puts a lower bound on the bandwidth of the closed loop system but also rejects high frequency noise. This rolls off frequency also limits the bandwidth to be well below Nyquist frequency of the controller. W_2 is a high pass filter designed to attenuate measurement noise. It rolls off at high frequency to reject noises from switching components. W_3 limits the magnitude of the input signal such that the output signal does not saturate. H_∞ controller will be simulated and implemented to both identified electrical and thermal systems.

4.1. H_∞ controller design of the electrical system and its implementation

The robust control for buck converter is designed with the goal to minimize tracking error and reject disturbance from the AC source. The disturbances of the systems can be contributed from noise from AC voltage source, the noise from switching mechanism of IGBT, electromagnetic interferences and sensor noise in measurements of v_s and i_o . $W_1 = \frac{0.1s + 375.1}{s + 0.3751}$ is designed such to have high amplitude of 40 dB at low frequency and roll off at higher frequency. This selection of W_1 yields minimized amplitude of $S(j\omega)$ at low frequency which can define the tracking error bandwidth. $W_2 = \frac{200(s + 1000)(s + 1300)}{(s + 6000)(s + 5500)}$ is designed to reject noises from switching components; mainly the switching frequency of the IGBT at 10 kHz. We designed $W_3 = 0.001$ to ensure that the current does not saturate.

The controller is found to be a 13th order transfer function. Balanced reduction [16] is used to obtain a 3rd order approximation

given by

$$K_E = \frac{28526(s + 1714)(s + 41.69)}{(s + 2132)(s + 61.58)(s + 0.375)} \quad (7)$$

The closed loop transfer function of linearized electrical system at the operating point is stable since all roots of the denominator in the closed loop transfer function are located on the left half plane at $-1382.51 \pm 709.83i$, $-1711.71 \pm 1016.06i$, $-397.27 \pm 61.37i$, -0.126 , and -430.83 , respectively.

The sensitivity and complementary sensitivity transfer functions S and T are shown in Fig. 8. The tracking performance is characterized by the -20 dB crossover frequency of S which is 200 Hz. The relatively low roll off frequency of T ensures mitigation of noise from the switching components at 10 kHz to -40 dB. The input signal in the simulation does not saturate at maximum duty cycle (100%), which is 2.51 A.

For implementation, the designed controller is converted from continuous to discrete time transfer function using Bilinear (Tustin) method. To ensure stability, reduce quantization effects of the computation, and perform parallel computation of the controller, the discretized controller is implemented as a biquad (second-order) IIR digital filter [17]. The implementation of the robust controller is implemented in FPGA with sampling time of 500 μ s. First order low pass filter of 10 kHz is also implemented on both i_o and V_s to reject sensor noises. In both measurements, two-element deep pipeline method is implemented to prevent data loss during signal processing [18].

Both closed loop frequency response from experiment and simulation of the electrical system are shown in Fig. 9. The -3 dB cut-off frequency of the closed loop transfer function is at 1527 rad/s (243 Hz). The closed loop bandwidth of the experiment shows slightly better noise mitigation at higher frequency. The sensitivity transfer function which can be used to determine the tracking bandwidth of both simulation and model have minimum peak values. Hence, the system is relatively robust to modelling uncertainties at the operating condition.

The closed-loop tracking performance from simulations and experiments are shown in Fig. 10. The transient response of the experiment of all three sets are similar. The parasitic resistances and inductances that are not included in the averaged model yields slightly different transient response. The steady state current of the proposed controller in the Buck converter circuit is found to be 0.3 ± 0.007 A. The response shows some oscillations especially at the steady state. This is mainly from the AC source as well as the noise due to switching from IGBT. The rise time of this closed loop-controlled response is 0.005 s, which is significantly faster than bandwidth of the thermal system. The step response performance is shown in Fig. 11. The steady-state tracking performance shows average root mean square error (RSME) of

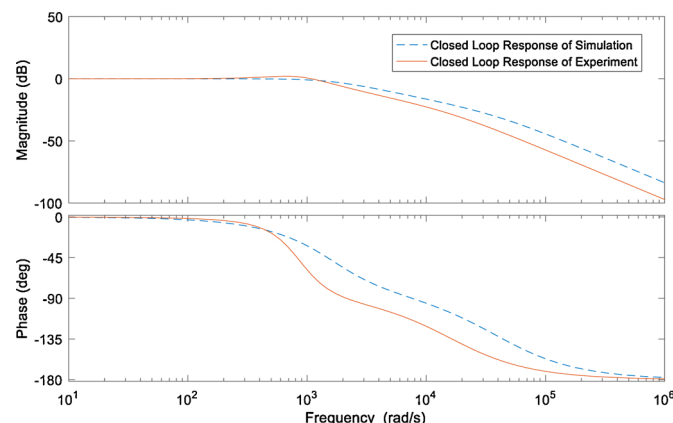


Fig. 9. Closed loop frequency response of electrical system from experiment and simulation.

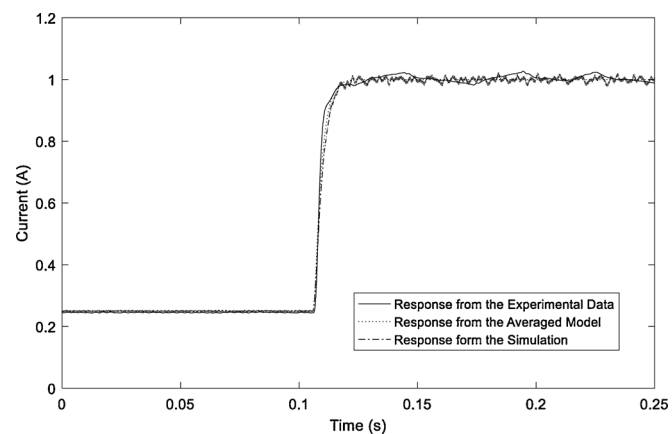


Fig. 10. Tracking performance results from simulation, averaged model and experiment.

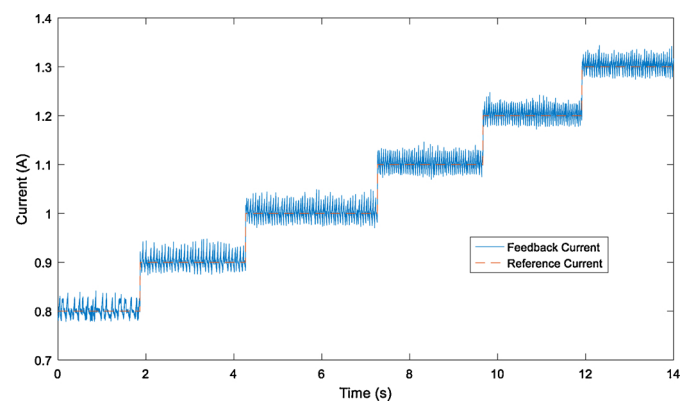


Fig. 11. Step response of the controller.

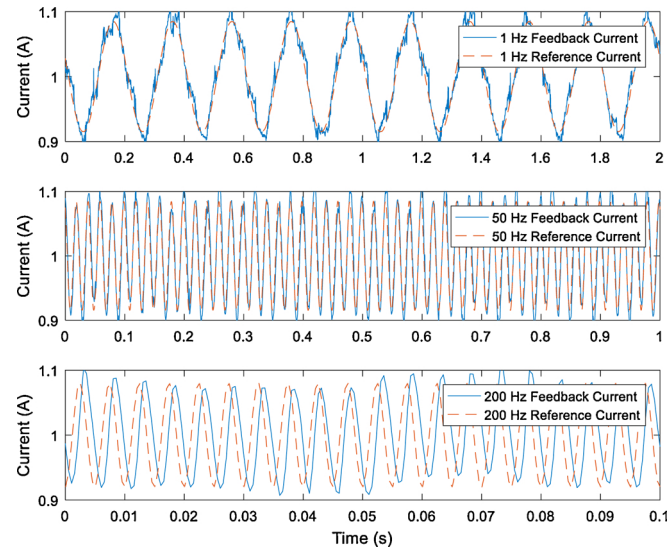


Fig. 12. Sinusoidal response of the electrical system.

0.012 A across all reference set points. Fig. 12 shows the tracking performance of the sinusoidal signal at frequency of 1 , 50 and 200 Hz providing RSME of 0.012 , 0.018 , and 0.0737 A, respectively. This controller can regulate rectified AC input and outputs current with a precision of less than 2% over a bandwidth of 5 Hz. Hence, this controller bandwidth of the electrical system is sufficient for the heater that has slower bandwidth of less than 0.1 Hz.

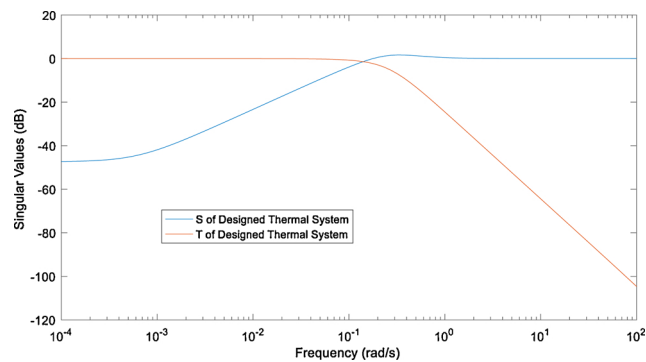


Fig. 13. S and T transfer function of thermal systems.

4.2. H_∞ controller design of the thermal system and its implementation

For temperature control design, we use similar design as for the electrical system (4.1) to regulate the temperature of the heater. The primary control design objectives are high precision temperature regulation, and robustness to external disturbances. The disturbances mainly include the effects of heat conduction to the testbed, convection to the air and noises from RTD. The weighting functions, W_1 , W_2 and W_3 , are designed as: $W_1 = \frac{0.0001s + 0.06283}{s + 6.283E - 6}$, $W_2 = \frac{10(s + 20.94)}{(s + 62.83)}$, $W_3 = \frac{20(s + 6.283e05)}{(s + 1.257e04)}$. The H_∞ controller from a similar design as for the electrical system is;

$$K_T = \frac{-0.00063272(s - 49.01)(s + 0.467)(s + 0.001164)}{(s + 2.559)(s + 0.3964)(s + 6.283e - 06)}. \quad (8)$$

The sensitivity and complementary sensitivity transfer functions S and T of the designed thermal system are shown in Fig. 13. The tracking performance is characterized by the -20 dB crossover frequency of S which is 0.1 rad/s (0.016 Hz). Similar to the electrical system design, the peak of S is minimized so that it is robust to modelling uncertainties at the operating condition. The roll off frequency of T is -40 dB at 20 rad/s (3.2 Hz) to attenuate the disturbance noise.

The closed loop transfer function of linearized thermal system at the operating point is stable since all roots of the denominator in the closed loop transfer function are located on the left half plane at $-0.095 \pm 0.067i$, $-0.12 \pm 0.36i$, -2195.14 , -0.029 , -0.085 , -2.81 and -2.91 , respectively.

The complementary sensitivity transfer function of the simulation and the experimental data shown in Fig. 14 match quite well up to 2 rad/s. The -3 dB cut-off frequency is at 0.15 Hz. The tracking performance of can be seen from the -20 dB crossover frequency of S which is 0.016 Hz. The -3 dB cut-off frequency is 1.6 Hz.

The proposed controller is converted from continuous to discrete

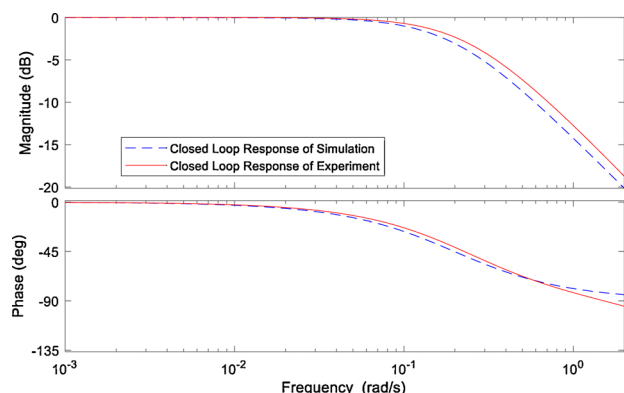


Fig. 14. Closed loop frequency response of thermal system from experiment and simulation.

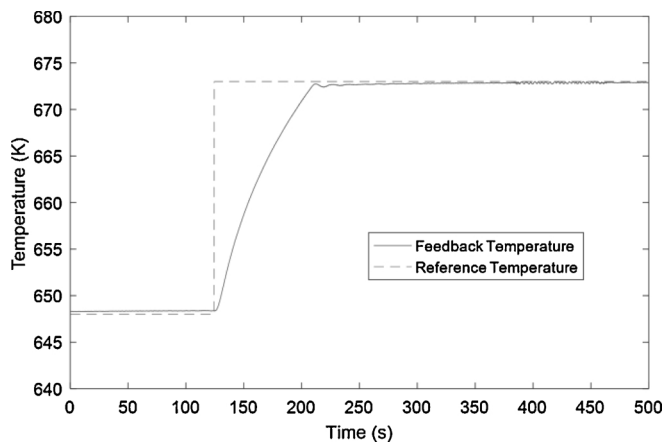


Fig. 15. Transient and steady-state performance comparison of the proposed controller.

time using bilinear transformation. The implementation of the robust controller of the heater is implemented in RT with sampling time of 10 ms. The transient response from 648 K to 673 K temperature reference is shown in Fig. 15. This robust controller in a proposed control framework shows that the temperature can be accurately regulated. The steady state temperature of the proposed controller in the buck converter circuit is found to be 672.9 ± 0.03 K, 648.1 ± 0.03 K, and 697.9 ± 0.02 K for reference temperature of 673 K, 648 K and 698 K respectively. Since only steady state, and robustness to disturbances of the temperature control are the main objectives in the study, the performance of the transient response is not significant.

As shown in Fig. 15, the tracking of temperature away from the operating point would deviate slightly as seen in the steady-state tracking of 648 K. The temperature range of 20 K is suitable for thermoplastic forming application. Fig. 16 shows the tracking performance of the sinusoidal signal at frequency of 0.01 , 0.1 Hz. At 0.01 Hz, the tracking performs well but the phase lag starts appearing when the frequency is increased as seen in 0.1 Hz case. For out application this is above the design specifications since only steady state temperature is significant.

4.3. Stability of the closed loop system

The stability analysis of the combined closed loop system is addressed. Both closed loop systems are locally stable from the controller design in 4.1 and 4.2. The stability of these two interconnected systems can be analysed using singular perturbation addressed in Section 3.2. The fast electrical system has bandwidth, ω_E on the order of several

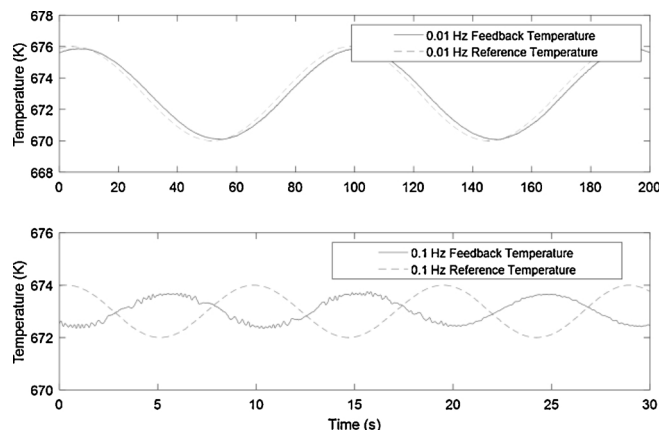


Fig. 16. Sinusoidal response of the thermal system.

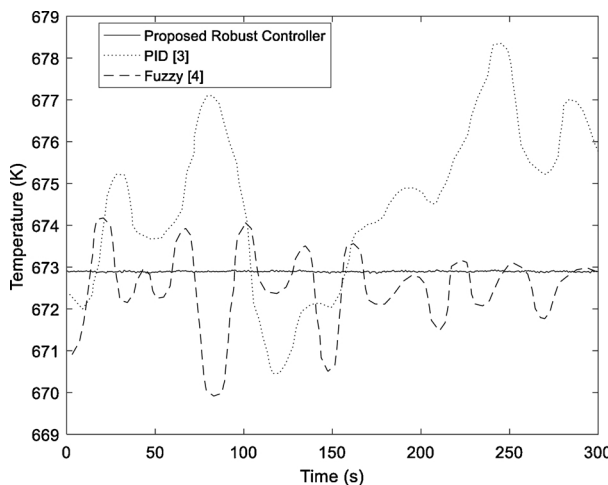


Fig. 17. Tracking performance comparison of the temperature from 3 controllers.

1000 rad/s. The slow thermal system has closed loop bandwidth, ω_T on the order of 0.1 rad/s. After obtaining the closed loop dynamics of both slow and fast system, Lemma 2.2 from [19] can be applied under condition of (3) and (4). $\frac{\omega_T}{\omega_E} < 1.58 \times 10^{-4}$ which is sufficiently small as the assumption made in 3.2. This verifies that the separate tuning of two robust controllers are feasible.

The proposed combined system can successfully convert rectified AC electrical power to regulate the temperature of the heater. The input and outputs current with a precision of 2 % over a bandwidth of 5 Hz. The temperature control design achieves the required temperature regulation at 673 K within 0.003 K at steady state. The proposed controller regulates the temperature of BMG sample and ensure that the viscosity of the BMG sample during thermoplastic drawing is within less than 2 % [2,3] of the desired value during the process. More consistent thermoplastic forming behaviour is seen in the process resulting in blades with better edges. Our design with better tracking bandwidth and accuracy enables techniques that are not possible previously; for instance, it can improve the quality of the blades by maintaining varying molding temperature along the drawing length of the blades. It could also be used in thermal forming processes such as glass forming and hot-wire cutting process [20].

5. Performance comparison with other controllers

The proposed controller is then compared with PID [3], and ARX based fuzzy logic controller [4]. Fig. 17 shows the performance comparison between all 3 controllers tracking the reference temperature at 673 K over 300 s. PID controller tracks at 674.8 ± 3.7 K and the ARX based fuzzy logic controller tracks at 672.5 ± 2.2 K. The proposed buck converter circuit tracks at 672.9 ± 0.03 K. It is noted that the tracking performance of proposed controller is more than 5000 % better than the performance of first 2 implemented controllers. This is due to the addition of H_∞ robust control and buck converter, which allow the controller to be design over both linearized electrical and thermal systems. The controlled current passing through the heater is also continuous in nature making the heater to be highly efficient and accurate.

The consistent temperature in the heating module of the testbed would sustain the temperature of BMG sample better thereby producing better quality blade edges. In addition, it requires a smaller number of components to manufacture the circuit compared to TRIAC phase angle control. The utilization of the AC and Buck converter helps reduce the setup cost and complication of the DAQ that does not require zero crossing detection from the optocoupler.

6. Conclusion

The new control architecture consisting of the design, identification, simulation, and control of a buck converter is implemented for BMG thermoplastic micro-forming is presented. Frequency-based system identification is performed on both the buck converter and the heater systems. A nested inner-current outer-temperature control system for high-fidelity temperature regulation is constructed. The inner-current control loop, which is implemented on a modified buck converter, allows high-power rectified AC input and outputs current to be regulated. The switch-averaged electrical model together with feedback linearization is used to overcome nonlinear dynamics embed in the buck converter. The required power input for the heater computed by slower the outer-loop control is translated to the corresponding reference with a bandwidth of over 1500 times faster than the thermal systems. This enables us to design control law for each loop separately. The control objectives of regulating the robustness to uncertainties and performance of the controller are solved in an optimal control (H_∞) framework and implemented on the hardware. The following conclusions can be drawn from this work:

- 1 The proposed electrical system control design regulates rectified AC input and outputs current with a precision of 2 % over a bandwidth of 5 Hz.
- 2 The set-up cost of this buck converter circuit system is relatively low compared to other existing approaches.
- 3 The temperature control design achieves the required temperature regulation at 673 K within 0.03 K at steady-state.
- 4 An improvement of over 5000 % is shown when compared with previously implemented control designs.
- 5 By regulating the temperature of BMG sample and ensure that the viscosity of the BMG sample during thermoplastic drawing is within less than 2 % of the desired value during the process [2,3]. As a result, more consistent thermoplastic forming behaviour can be performed and manufacture good edge blades.

Declaration of Competing Interest

The authors declare that they have no known competing financial interests or personal relationships that could have appeared to influence the work reported in this paper

References

- [1] Liu L, Qiu CL, Huang CY, Yu Y, Huang H, Zhang SM. Biocompatibility of Ni-free Zr-based bulk metallic glasses. *Intermetallics* 2009;17(4):235–40.
- [2] Krejcie Alexander, Kapoor Shiv G, Devor Richard E. A hybrid process for manufacturing surgical-grade knife blade cutting edges from bulk metallic glass. *J Manuf Process* 2012;14:26–34.
- [3] Zhu James, Kapoor Shiv. Development of a hybrid thermoplastic forming process for the manufacture of curvilinear surgical blades from bulk metallic glass. *ASME J Micro Nano-Manuf* 2017;5(1):1103.
- [4] Dancholvichit Nattasit, Kapoor Shiv G. An ARX-based temperature controller for a hybrid thermoplastic micro-forming of surgical blades from bulk metallic glass. *J Micro Nano-Manuf* 2020;8(3).
- [5] Liu Tao, Yao Ke, Gao Furong. Identification and autotuning of temperature-control system with application to injection molding. *IEEE Trans Control Syst Technol* 2009;17(6):1282–94.
- [6] Zhang Junming, Zeng Hulong, Jiang Ting. A primary-side control scheme for high-power-factor LED driver with TRIAC dimming capability. *IEEE Trans Power Electron* 2012;27(11):4619–29.
- [7] Liu Hao, Wang Jihong. Analysis and control of a single phase AC chopper in series connection with an auto-transformer. 18th international conference on automation and computing (ICAC). 2012.
- [8] Moon Sang Cheol, Chung BongGeun, Koo Gwanbon, Guo Jason, Balogh Laszlo. A conduction band control AC-DC Buck converter for a high efficiency and high power density adapter. 2017 IEEE applied power electronics conference and exposition (APEC) 2017.
- [9] Baharom R, Hashim H, Seroji MN, Hamzah MK. A new single-phase controlled rectifier using single-phase matrix converter. 2006 IEEE international power and energy conference 2006.
- [10] Dudrik Jaroslav, Trip Nistor-Daniel. Soft-switching PS-PWM DC-DC converter for

- full-load range applications. *IEEE Trans Ind Electron* 2009;57(8):2807–14.
- [11] Lauritzen Peter O, Andersen Gert K, Helsper Martin. A basic IGBT model with easy parameter extraction. 2001 IEEE 32nd annual power electronics specialists conference (IEEE Cat. No. 01CH37230) 2001;IEEE Vol. 4.
- [12] Middlebrook Richard D, Cuk Slobodan. A general unified approach to modelling switching-converter power stages. 1976 IEEE power electronics specialists conference. 1976.
- [13] Li Lijie, Chew Zheng J. Microactuators: design and technology. Smart sensors and MEMS. Woodhead Publishing; 2018. p. 313–54.
- [14] Khalil Hassan K, Grizzle Jessy W. Nonlinear systems Vol. 3. Upper Saddle River, NJ: Prentice hall; 2002.
- [15] Mohan Ned, Undeland Tore M, Robbins William P. Power electronics: converters, applications, and design. John Wiley & Sons; 2003.
- [16] Skogestad S, Postlethwaite I. Multivariable feedback control: analysis and design. New York: Wiley; 2007.
- [17] Oppenheim AV, Schafer RW. Digital signal processing. Englewood Cliffs, NJ: Prentice-Hall; 1975.
- [18] NI 9205 - Products and Services - National Instruments, National Instruments Corp, <http://sine.ni.com/nips/cds/view/p/lang/en/nid/202571>.
- [19] Kokotovic Petar, Khalil Hassan K, O'reilly John. Singular perturbation methods in control: analysis and design Vol. 25. Siam; 1999.
- [20] Abeyasinghe Asith, Abeywardena Shameera, Nanayakkarasam Roshan, Wimalsiri Walallawita, Dulantha Lalitharatne Thilina, Tennakoon Salinda. Development of a numerically controlled hot wire foam cutting machine for wing mould construction. 2016 Moratuwa engineering research conference (MERCon) 2016.